https://doi.org/10.1093/plcell/koac334 THE PLANT CELL 2023: 35: 700–716

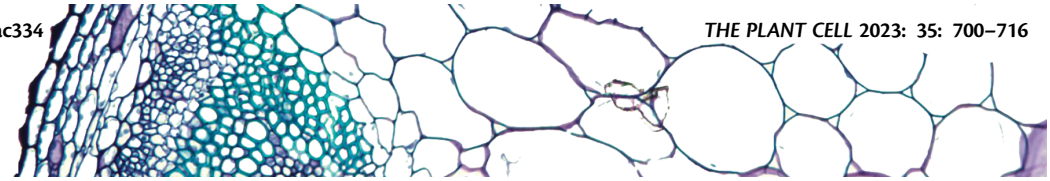

Research Article

The noncoding RNA *HIDDEN TREASURE 1* promotes phytochrome B-dependent seed germination by repressing abscisic acid biosynthesis

Yuqiu Wang [1,†] **Yangyang Fan** [1,†,‡] **De Fan** [1,2,†] **Xiaoli Zhou** [1] **Yuntong Jiao** [1] **Xing Wang Deng** [1,2,*] **and Danmeng Zhu** [1,*]

1 State Key Laboratory of Protein and Plant Gene Research, School of Advanced Agricultural Sciences and School of Life Sciences, Peking-Tsinghua Center for Life Sciences, Peking University, Beijing 100871, China
2 Peking University Institute of Advanced Agricultural Sciences, Shandong Laboratory of Advanced Agricultural Sciences in Weifang, Weifang, Shandong 261325, China

*Author for correspondence: zhudanmeng@pku.edu.cn (X.W.D), deng@pku.edu.cn (D.Z.)
†These authors contributed equally to this work.
‡Present address: Institute of Plant Protection, Beijing Academy of Agriculture and Forestry Sciences, Beijing Engineering Research Center for Edible Mushroom, 9 Shuguang Garden Zhonglu, Haidian District, Beijing 100097, China

Y.W., X.W.D., and D.Z. designed the research; Y.W. performed most experiments; Y.W. and Y.F. carried out all -omics data analysis; D.F. performed the in situ hybridization assays and generated parts of the constructs; X.Z generated parts of the genetic material; Y.J. performed parts of the RNA imaging analysis; Y.W., X.W.D., and D.Z. analyzed the data; and Y.W., D.F., X.W.D., and D.Z. wrote the paper.
The authors responsible for distribution of materials integral to the findings presented in this article in accordance with the policy described in the Instructions for Authors (https://academic.oup.com/plcell/pages/General-Instructions) are: Danmeng Zhu (zhudanmeng@pku.edu.cn) and Xing Wang Deng (deng@pku.edu.cn).

Abstract

Light is a major environmental factor for seed germination. Red light-activated phytochrome B (phyB) promotes seed germination by modulating the dynamic balance of two phytohormones, gibberellic acid (GA) and abscisic acid (ABA). How phyB modulates ABA biosynthesis after perceiving a light signal is not yet well understood. Here, we identified the noncoding RNA *HIDDEN TREASURE 1* (*HID1*) as a repressor of ABA biosynthesis acting downstream of phyB during *Arabidopsis thaliana* seed germination. Loss of *HID1* function led to delayed phyB-dependent seed germination. Photoactivated phyB promoted the accumulation of *HID1* in the radicle within 48 h of imbibition. Our transcriptomics analysis showed that *HID1* and phyB co-regulate the transcription of a common set of genes involved in ABA and GA metabolism. Through a forward genetic screen, we identified three ABA biosynthesis genes, *ABA DEFICIENT 1* (*ABA1*), *ABA2*, and *ABA3*, as suppressors of *HID1*. We further demonstrated that *HID1* directly inhibits the transcription of *9-CIS-EPOXYCAROTENOID DIOXYGENASE* (*NCED9*), a gene encoding a key rate-limiting enzyme of ABA biosynthesis. *HID1* interacts with ARABIDOPSIS TRITHORAX-RELATED7 (ATXR7), an H3K4me3 methyltransferase, inhibiting its occupancy and H3K4me3 modification at the *NCED9* locus. Our study reveals a nuclear mechanism of phyB signaling transmitted through *HID1* to control the internal homeostasis of ABA and GA, which gradually optimizes the transcriptional network during seed germination.

Introduction

Seeds monitor the environment in order to germinate at the optimal time, which is a life-or-death decision, and selecting the right moment is crucial for subsequent robust seedling establishment. Seed germination is affected by numerous environmental factors including light, temperature, humidity, and nutrition (Weitbrecht et al., 2011). The phytohormones gibberellic acid (GA) and abscisic acid (ABA) are major

Received June 09, 2022. Accepted November 05, 2022. Advance access publication November 25, 2022

internal signaling molecules that play central roles in the regulation of seed germination (Seo et al., 2009). Seed germination is promoted by decreased ABA levels and increased GA levels (Seo et al., 2006); therefore, the balance between these two antagonistic hormones determines the capacity of a seed for germination (de Wit et al., 2016).

Light is a critical factor during seed germination (Borthwick et al., 1952). It is well acknowledged that the phytochrome photoreceptors play important roles in light-initiated seed germination. In *Arabidopsis thaliana*, five genes (*phyA* to *phyE*) encode phytochromes, among which phyA and phyB play dominant roles in the regulation of seed germination (Shinomura et al., 1994; 1996). phyB mediates red light-induced seed germination, whereas phyA triggers canopy light-induced seed germination (Lee et al., 2012). Upon red light irradiation, photoactivated phyB directly interacts with PHYTOCHROME INTERACTING FACTOR 1 (PIF1), a negative regulator of seed germination, leading to the rapid phosphorylation and degradation of PIF1 via the 26S proteasome (Oh et al., 2004; 2006). The phyB–PIF1 de-repression module ultimately promotes increased levels of GA and reduced levels of ABA, facilitating seed germination (Oh et al., 2007; Kim et al., 2008; Cho et al., 2012; Shi et al., 2013; 2015). Subsequently, the phyB–FHY3 (FAR-RED ELONGATED HYPOCOTYL 3) interaction further increases the levels of bioactive GA to promote germination (Jiang et al., 2016; Yang et al., 2020; Liu et al., 2021). It is well-established that ABA levels in imbibed seeds decrease dramatically after exposure to red light; however, little is known regarding the link between phyB and the genes involved in ABA biosynthesis, through which phyB activation promotes seed germination during prolonged imbibition.

Recent genome-wide profiling data sets have shown that noncoding RNAs (ncRNAs) occupy a significant portion of the transcriptome in eukaryotes (Berretta and Morillon, 2009; Mattick et al., 2010). Increasing evidence indicates that ncRNAs regulate gene expression at both the transcriptional and post-transcriptional levels. Long noncoding RNAs (lncRNAs), which are longer than 200 nucleotides (nts), comprise a sizable set of ncRNAs that perform diverse functions in vivo (Statello et al., 2021). In plants, thousands of lncRNAs have been identified or predicted, but only a few have been fully functionally characterized (Wang and Chekanova, 2017). Recent studies have begun to uncover the regulatory role of nucleus-localized lncRNAs that associate with chromatin and regulate gene transcription at the nexus of environmental responses and plant development (Yu et al., 2019). Several studies suggest that certain microRNAs, including miR163 (Chung et al., 2016), miR390 (Sarkar Das et al., 2018), and miR408 (Jiang et al., 2021), play a role in the control of seed germination; however, the functions of lncRNAs in seed germination remain largely elusive.

Our previous studies have revealed that *HIDDEN TREASURE 1* (*HID1*), a conserved 236-nt noncoding RNA in the plant kingdom, acts as a chromatin-bound lncRNA and directs transcriptional regulation underlying light-dependent seedling development (Wang et al., 2014a, 2014b; 2018a, 2018b). In the present study, we identified *HID1* as a positive regulator of phyB-dependent seed germination. *HID1* acts genetically downstream of phyB. The expression of *HID1* is gradually enriched in the radicle during seed germination in a phyB-dependent manner. The phyB-*HID1* axis modulates the expression of genes involved in ABA and GA metabolism and signaling after 24 h of imbibition. The results of our molecular and forward genetic analyses suggest that *HID1* promotes phyB-mediated seed germination predominantly by repressing ABA biosynthesis. *HID1* directly represses the transcription of *NCED9*, a gene encoding a key ABA biosynthesis enzyme, and inhibits the occupancy of ATXR7 at *NCED9*. Therefore, our study uncovers another layer of phyB-dependent regulation of seed germination mediated by a lncRNA, which converts external light signals into internal phytohormone signaling to promote seed germination.

Results

HID1 acts as a positive regulator of phyB-dependent seed germination

To identify ncRNAs that function during red light-induced seed germination in *Arabidopsis thaliana*, we utilized the phyB-dependent germination protocol (Shi et al., 2013) and screened a collection of *Agrobacterium tumefaciens*-transferred DNA (T-DNA) insertion mutants that were compromised in the expression of specific ncRNAs for delayed or accelerated seed germination phenotypes. In principle, seeds were exposed to far-red light (5 μmol m^{-2} s^{-1}) followed by red light (20 μmol m^{-2} s^{-1}), before incubation in the dark for five days (phyB-on conditions) (Figure 1A).

In the screening, the ncRNA mutant *hidden treasure 1* (*hid1*) exhibited a reduced germination rate during phyB-dependent seed germination (Figure 1B). The germination rate of wild-type (WT) seeds was roughly 80% following 48 h dark incubation after light treatment (DAL), and this rate gradually increased to almost 100% during prolonged dark incubation. However, the *hid1* mutants did not germinate following 48 h DAL. After 5 days of DAL, only ~70% of the *hid1* mutant seeds had germinated, while WT seeds had a germination frequency of almost 100%. Under phyB-off conditions, during which phyB is inactive, neither WT nor *hid1* seeds germinated (Supplemental Figure S1, A and B).

In a previous study, we showed that the T-DNA insertion of the *hid1* mutant used in these experiments occurs upstream of a polycistronic ncRNA cluster including *HID1*, causing a dramatic reduction in the expression of all four ncRNAs (Wang et al., 2014a, 2014b). Expression of *HID1* under the control of its endogenous promoter in the *hid1* background (*pHID1:HID1/hid1*) rescued the elongated hypocotyl phenotype of *hid1* to that of WT (Wang et al., 2014a, 2014b). In the present study, we observed that the germination rate of *pHID1:HID1/hid1* seeds was comparable to that of WT seeds (Figure 1, B, and C). Considering that ~60% of *hid1*

seeds germinated at 48 h under white light (WL) after 3 days of cold stratification (Supplemental Figure S1, C and D), but *hid1* seeds had not germinated at all following 48 h DAL under phyB-on conditions, these results indicate that *HID1* acts as a positive regulator of phyB-mediated seed germination. We also tested whether *HID1* is involved in phyA-mediated seed germination. Following 96 h and 120 h of DAL under phyA-on conditions, during which phyA is activated by a second far-red irradiation after 48 h dark treatment, the *hid1* mutants had a lower seed germination rate than WT (Supplemental Figure S1, E and F), suggesting that *HID1* plays a role in phyA-dependent germination.

Next, to determine whether *HID1* acts directly as a bona fide ncRNA in seed germination, we took advantage of our previously generated transgenic lines expressing mutated *HID1* to predict the *HID1* open-reading frame in the *hid1* mutant: (1) Mut1, mutation of ATG to ATA; and (2) Mut2, deletion of ATG to AG (Wang et al., 2014a, 2014b). As expected, the two transgenic lines phenocopied the WT under phyB-on conditions (Figure 1, D and E), suggesting that *HID1* functions as a noncoding RNA to promote red light-induced seed germination.

Our previous study showed that two stem loops of *HID1*, SL2, and SL4, are essential for *HID1*-mediated hypocotyl elongation under continuous red light; therefore, we evaluated their importance in *HID1*-regulated seed germination. We examined the germination rate of WT, *hid1*, and transgenic lines expressing *HID1* mutants that lack SL2 or SL4 in the *hid1* mutant background under phyB-on conditions. These mutants had a germination rate similar to that of *hid1* mutants, indicating that SL2 and SL4 are essential for *HID1*-mediated seed germination (Figure 1F).

To assess whether the function of *HID1* in phyB-dependent seed germination is conserved among monocots and dicots, we examined the seed germination rate of WT, *hid1*, and transgenic lines expressing the rice (*Oryza sativa*) *HID1* homolog, *OsHID1*, driven by the *OsHID1* endogenous promoter in the *hid1* background (Wang et al., 2014a, 2014b). Following 24 h DAL, *OsHID1* transgenic seeds had a consistently higher germination rate than that of the *hid1* mutants under phyB-on conditions (Figure 1G), suggesting that the functions of *AtHID1* and *OsHID1* may be conserved in phyB-dependent seed germination. Taken together, these results suggest that being a noncoding RNA, *HID1* promotes light-dependent seed germination.

phyB promotes the accumulation of *HID1* in radicles

To examine the spatial expression pattern of *HID1* during seed germination under phyB-on conditions, we used a *pHID1:GUS* reporter construct to study *HID1* promoter activity in stable transgenic plants. Interestingly, the *HID1* promoter is primarily active in the embryo and is highly active in the radicle following 48 h DAL (Figure 2A). Under phyB-off conditions, during which phyB is inactivated by illumination with far-red light, the *HID1* promoter was almost inactive following 48 h DAL. These results suggest that expression of the *HID1* promoter in the radicle is modulated by phyB during seed germination.

Next, we performed in situ hybridization to investigate the expression of *HID1* in imbibed seeds of the WT and *phyB* lines following 12, 24, and 48 h DAL under phyB-on conditions. In embryos from both WT and *phyB* mutant seeds, the expression of *HID1* displayed a dispersed pattern at 12 h and 24 h under phyB-on conditions (Figure 2B). Similar to our observation of *HID1* promoter activity (*pHID1:GUS*), *HID1* was mainly expressed in the radicle following 48 h DAL (Figure 2B); however, loss of *phyB* abolished the expression of *HID1* in the radicle following 48 h DAL (Figure 2B), suggesting that phyB promotes the accumulation of *HID1* in the radicle during seed germination. Furthermore, RNA gel blotting showed that *HID1* was constantly expressed in imbibed WT seeds during seed germination, and its expression was not obviously affected in *phyB* (Figure 2C). To precisely examine the changes in *HID1* expression in the radicle of imbibed seeds, we generated a transgenic line expressing *pHID1:GUS* in the *phyB* mutant. We assessed the expression levels of *β-glucuronidase* (*GUS*) and endogenous *HID1* in the radicle and non-radicle cells of *pHID1:GUS*/WT and *pHID1:GUS*/*phyB* seeds following 48 h DAL. RT-qPCR demonstrated that both *GUS* and *HID1* had significantly elevated expression levels in the radicle of the *pHID1:GUS*/WT line as compared with non-radicle cells; however, in *pHID1:GUS*/*phyB* seeds, *GUS* and *HID1* had similar expression levels in radicle and non-radicle cells (Figure 2D). Taken together, these data suggest that phyB promotes the accumulation of *HID1* in the radicle during seed germination.

To further examine the subcellular localization of *HID1* in vivo, we applied the RNA aptamer Broccoli to the RNA imaging of *HID1* (Filonov et al., 2014). It has been reported that Broccoli gives rise to a fluorescence signal at 507 nm following excitation in the appropriate working solution supplemented with the chemical compound DFHBI-1 T. We generated stable transgenic lines expressing *pHID1:Broccoli-HID1* in *hid1* (Supplemental Figure S2A). Our genetic and phenotypic analyses showed that a high expression level of *Broccoli-HID1* fully rescued the delayed germination phenotype of *hid1* to that of WT under phyB-on conditions (Supplemental Figure S2B).

To better assess the nuclear localization of *HID1*, we introduced the nuclear marker *35S:mCherry-SV40-NLS* into the *pHID1:Broccoli-HID1* line. *In vivo* imaging of *HID1* in the root tip of WL-grown seedlings (initiated with their roots in DFHBI-1 T solution) showed that the fluorescence signal of *Broccoli-HID1* clearly overlapped with that of mCherry-SV40-NLS (Supplemental Figure S2, C and D), supporting our previous finding that *HID1* is primarily nucleus-localized. Taking advantage of this *Broccoli*-tagged *HID1* transgenic line, we found that *HID1* was also enriched in the nuclei of radicle cells following 48 h DAL (Figure 2E), although the nuclear marker mCherry-SV40-NLS was expressed at low levels at this stage. Taken together, these results suggest that *HID1* is gradually enriched in the radicle and nucleus-localized under phyB-on conditions.

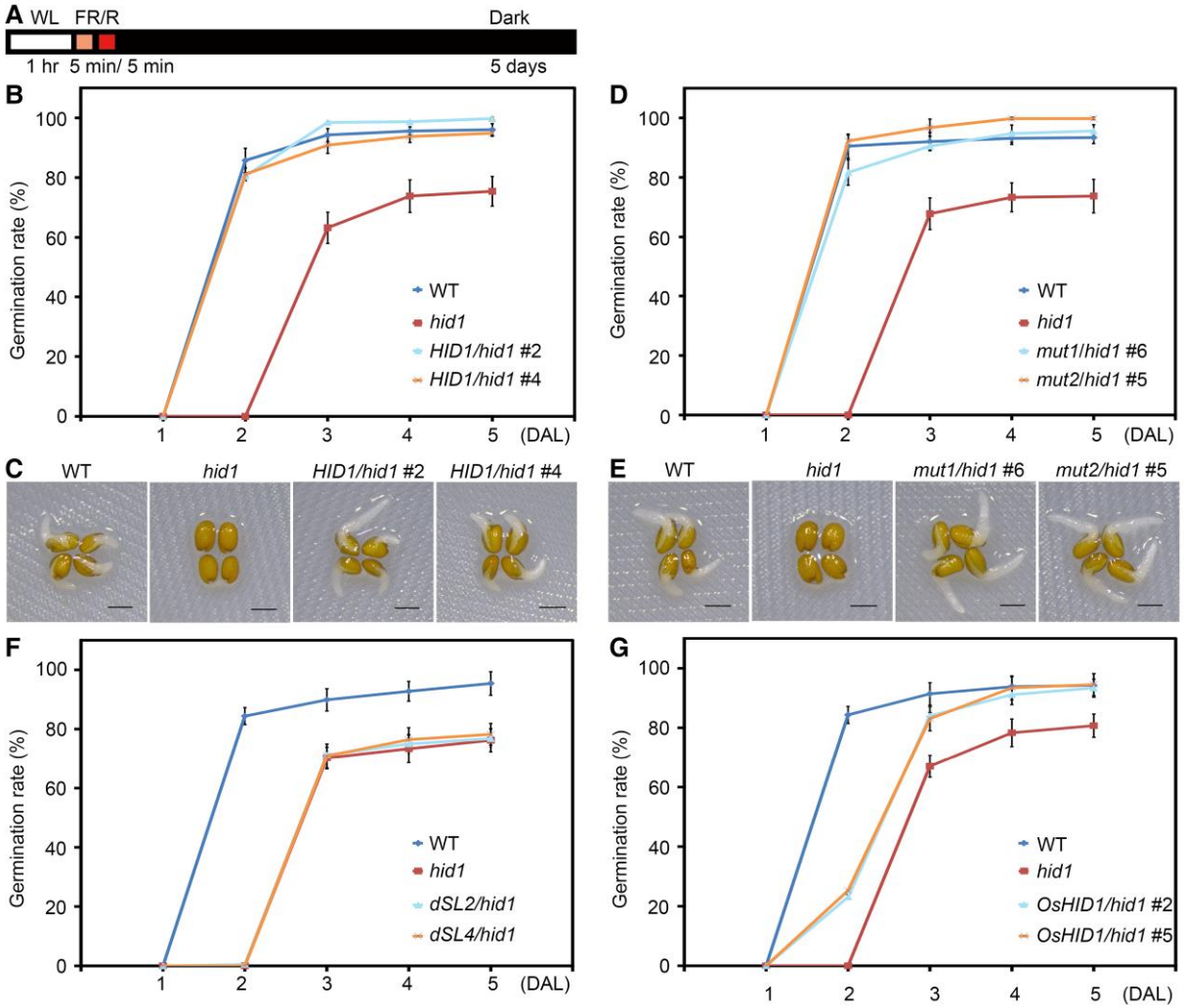

Figure 1 The ncRNA mutant *hid1* exhibits delayed germination under phyB-on conditions. A, Schematic illustration of phyB-on conditions. Seeds were exposed to continuous WL (50 μmol m^{-2} s^{-1}) for 1 h before exposure to far-red light (FR) (5 μmol m^{-2} s^{-1}) for 5 min (min) to inactivate phyB. The seeds were then irradiated with red light (R) (20 μmol m^{-2} s^{-1}) for 5 min to activate phyB before incubation in the dark for the indicated time (5 days). B, Germination rates of WT, *hid1*, and *pHID1:HID1/hid1* (*HID1/hid1*) seeds under phyB-on conditions. Germination rates were recorded every 24 h after light treatment. Mean ± standard deviation (SD), $n = 3$. C, Representative images of WT, *hid1*, and *HID1/hid1* seeds at 48 h under phyB-on conditions. Scale bar, 1 mm. D, Germination rates of WT, *hid1*, *mut1/hid1*, and *mut2/hid1* seeds under phyB-on conditions. Mean ± SD, $n = 3$. E, Representative images of WT, *hid1*, *mut1/hid1*, and *mut2/hid1* seeds at 48 h under phyB-on conditions. Scale bar, 1 mm. F, Germination rates of WT, *hid1*, *dSL2/hid1*, and *dSL4/hid1* seeds under phyB-on conditions. Mean ± SD, $n = 3$. G, Germination rates of WT, *hid1*, and *OsHID1/hid1* seeds under phyB-on conditions. Mean ± SD, $n = 3$.

HID1 and phyB co-regulate the expression of a large set of genes at 48 h under phyB-on conditions

To further explore the function of *HID1* in phyB-dependent seed germination, we incubated imbibed WT, *hid1*, and *phyB* seeds under phyB-on conditions and then sampled each group following 12, 24, and 48 h DAL for deep mRNA sequencing. Differentially expressed genes (DEGs; *phyB*/WT, *hid1*/WT, q value <0.05, fold change >1.5) were selected for further analysis (Supplemental Data Set 1). From the comprehensive transcriptomics analysis, we observed that a significant portion of the transcriptome was regulated by phyB during the three selected time points (Figure 3, A–C). In total, the *phyB*/WT comparison yielded 8,539 DEGs following 12 h DAL and 17,341 DEGs following 48 h DAL. However, the *hid1*/WT comparison yielded only 975 DEGs following 12 h DAL and 12,027 DEGs following 48 h DAL (Figure 3, D–G). Interestingly, the differences in the transcriptome revealed by the *hid1*/WT and *phyB*/WT comparisons were similar following 48 h DAL under phyB-on conditions (Figure 3, H and I). Two sets of DEGs, comprising 2,825 co-upregulated DEGs and 7,153 co-downregulated DEGs, accounted for more than half of the *phyB*-regulated genes and more than 80% of the *hid1*-regulated genes, indicating that *phyB* and *HID1* co-regulate a large set of genes following 48 h DAL. Similarly, the expression levels of most of the *hid1*- and *phyB* DEGs were not highly correlated following

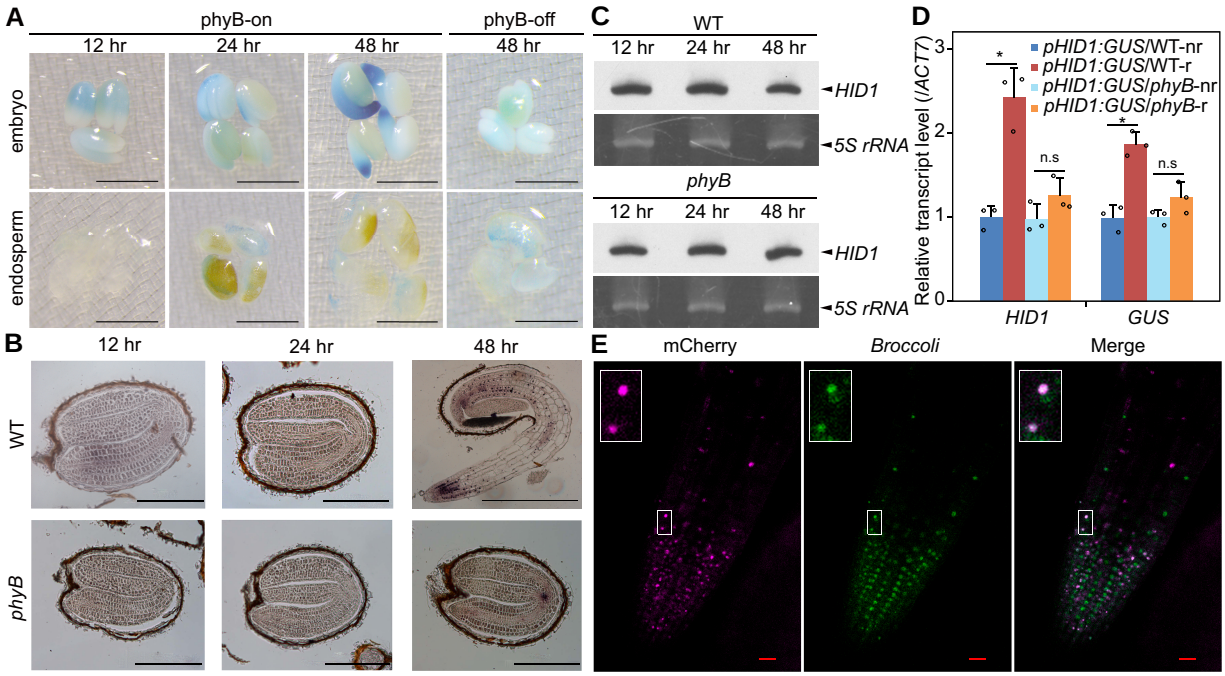

Figure 2 PhyB promotes nuclear accumulation of *HID1* in the radicle. A, GUS staining showing the expression pattern of *pHID1:GUS*/WT transgenic seeds under phyB-on and phyB-off conditions. Scale bar, 1 mm. B, *In situ* hybridization of WT and *phyB* seeds under phyB-on conditions with the *HID1* antisense probe. Scale bar, 0.5 mm. C, RNA gel blots showing the expression levels of *HID1* in WT and *phyB* seeds under phyB-on conditions. *5S rRNA* was used as the loading control. D, RT-qPCR showing the mRNA levels of *HID1* and *GUS* in the non-radicle (nr) and radicle (r) parts of *pHID1:GUS*/WT and *pHID1:GUS*/*phyB* transgenic seeds at 48 h under phyB-on conditions. Mean ± SD, $n = 3$. n.s, no significance. * $P \leq 0.05$ (two-tailed Student's *t*-test). E, RNA imaging of *Broccoli-HID1* in *Broccoli-HID1*/*hid1* seeds possessing the *35S:mCherry-SV40-NLS* cassette at 48 h after DAL under phyB-on conditions. Scale bar, 20 μm. An enlarged view of selected *Broccoli-HID1* and mCherry-SV40-NLS fluorescence signals are shown in the top left corner.

12 h or 24 h DAL (Figure 3, J–K), while their directions were highly correlated following 48 h DAL (R = 0.7866) (Figure 3L). This genome-wide analysis revealed that *HID1* regulates a subset of genes following 24 h DAL but mainly regulates gene expression following 48 h DAL, which is different from the rapid response mediated by PIF1.

It is well-established that the balance between signaling pathways activated by GA and ABA is an important regulator of seed germination, and it has been reported that phyB represses PIF1 following 12 h DAL to regulate the expression of many genes in the GA and ABA pathways. We chose several phyB–PIF1-regulated GA and ABA biosynthesis and metabolism genes as examples and measured their expression levels by RT-qPCR using total RNA samples extracted from the WT, *hid1*, *PIF1OX* (transgenic line overexpressing *PIF1*), and *phyB* lines following 12 h DAL. Consistent with previous studies, the levels of four genes, *9-CIS-EPOXYCAROTENOID DIOXYGENASE* (*NCED9*), *ABA INSENSITIVE 5* (*ABI5*), *SOMNUS* (*SOM*), and *REPRESSOR OF GA1–3* (*RGA*), were upregulated in the *phyB* mutant and *PIF1OX* lines as compared with those in the WT line following 12 h DAL (Supplemental Figure S3, A–C). Following 12 h DAL, the levels of *CYP707A2*, *EXPANSIN 8* (*EXP8*), and *EXP10* were downregulated in the *phyB* and *PIF1OX* lines (Supplemental Figure S3, A–C), but the expression levels of these genes were either unaffected or regulated in the opposite direction in the *hid1* line. Following 48 h DAL, the above-mentioned genes in ABA and GA metabolism were co-regulated by *HID1* and *phyB* (Supplemental Figure S3D). Taken together, these results indicate that *HID1* may not participate in phyB–PIF1-mediated rapid transcriptional regulation occurring within 12 h of seed imbibition.

The phyB-*HID1* axis regulates multiple phytohormones and cellular metabolism genes following 48 h DAL

To further decode the phyB-*HID1* regulatory network functioning during seed germination, we performed gene ontology (GO) analysis using the AgriGO software. Following 48 h DAL, the upregulated genes in the *phyB* and *hid1* lines were enriched in several GO terms: response to ABA stimulus, ABA metabolic processes, seed development, and response to water. In contrast, the downregulated genes were primarily enriched in two GO terms: response to hormone stimuli and cellular metabolism (Figure 4A).

Based on our time-course transcriptomics analysis, we further analyzed DEGs related to plant hormone regulation in the *hid1* and *phyB* mutants. In accordance with the results mentioned above, the expression levels of phytohormone

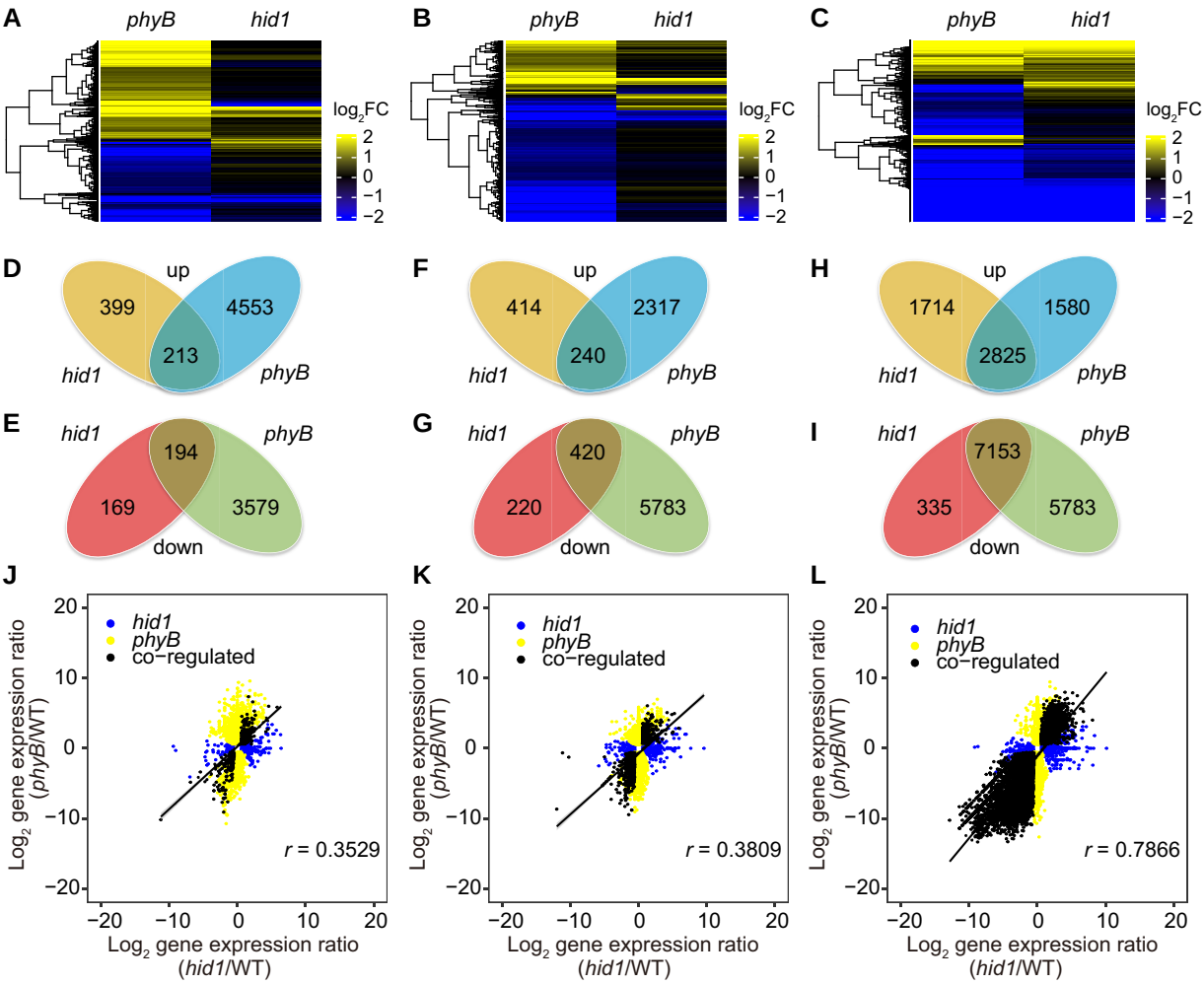

Figure 3 *HID1* and phyB co-regulate a large set of genes at the transcriptional level at 48 h under phyB-on conditions. A–C, Cluster analysis of *hid1*- and *phyB*-regulated genes following 12, 24, and 48 h DAL under phyB-on conditions. The scale bar shows the log2 transformation of the ratio. D, F, and H, Venn diagrams showing the overlap between *hid1*- and *phyB*-upregulated genes following 12, 24, and 48 h DAL under phyB-on conditions. E, G, and I, Venn diagrams showing the overlap between *hid1*- and *phyB*-downregulated genes following 12, 24, and 48 h DAL under phyB-on conditions. J, K, and L, Correlation scatterplots of the log2 fold change values between *hid1*- and *phyB*-regulated genes at 12, 24, and 48 h under phyB-on conditions.

metabolic and signaling genes were mostly unaffected in the *hid1* line following 12 h DAL, whereas they were mildly affected following 24 h DAL, suggesting that *HID1* plays a minor role in seed germination at these timepoints (Figure 4B). Following 48 h DAL, the expression levels of ABA biosynthesis genes, including *ABA1*, *NCED6*, and *NCED9*, as well as positive regulators of the ABA signaling pathway, including *ABI3* and *ABI5*, were co-upregulated in the *hid1* and *phyB* lines (Figure 4, C–H). The expression levels of GA biosynthesis genes, including *GA3OX1* and *GA3OX2*, as well as many other plant hormone-related genes, were downregulated in the *hid1* and *phyB* lines (Figure 4, I and J). In addition to ABA and GA, other plant hormones including cytokinin, auxin, brassinosteroids (BRs), ethylene, and jasmonic acid, have also been found to regulate seed germination. The temporal dynamics of the transcriptomics datasets of the WT line showed that the expression levels of ABA biosynthesis and signaling genes gradually decreased during seed germination under phyB-on conditions, while the expression levels of biosynthesis and signaling genes related to GA, BR, auxin, and cytokinin gradually increased (Figure 4B; and Supplemental Figure S4). Taken together, these results suggest that loss of *HID1* causes transcriptional reprogramming of the phytohormone network, promoting ABA signaling and inhibiting signaling downstream of GA and other germination-promoting phytohormones.

To further explore the genetic relationship between *HID1* and *phyB*, we crossed our previously generated *35S:HID1*/*hid1* line with the *phyB* single mutant to obtain a homozygous *35S:HID1*/*phyB* transgenic line. Overexpression of *HID1* alleviated the seed germination defect of *phyB* mutants under phyB-on conditions (Supplemental Figure S5A). We

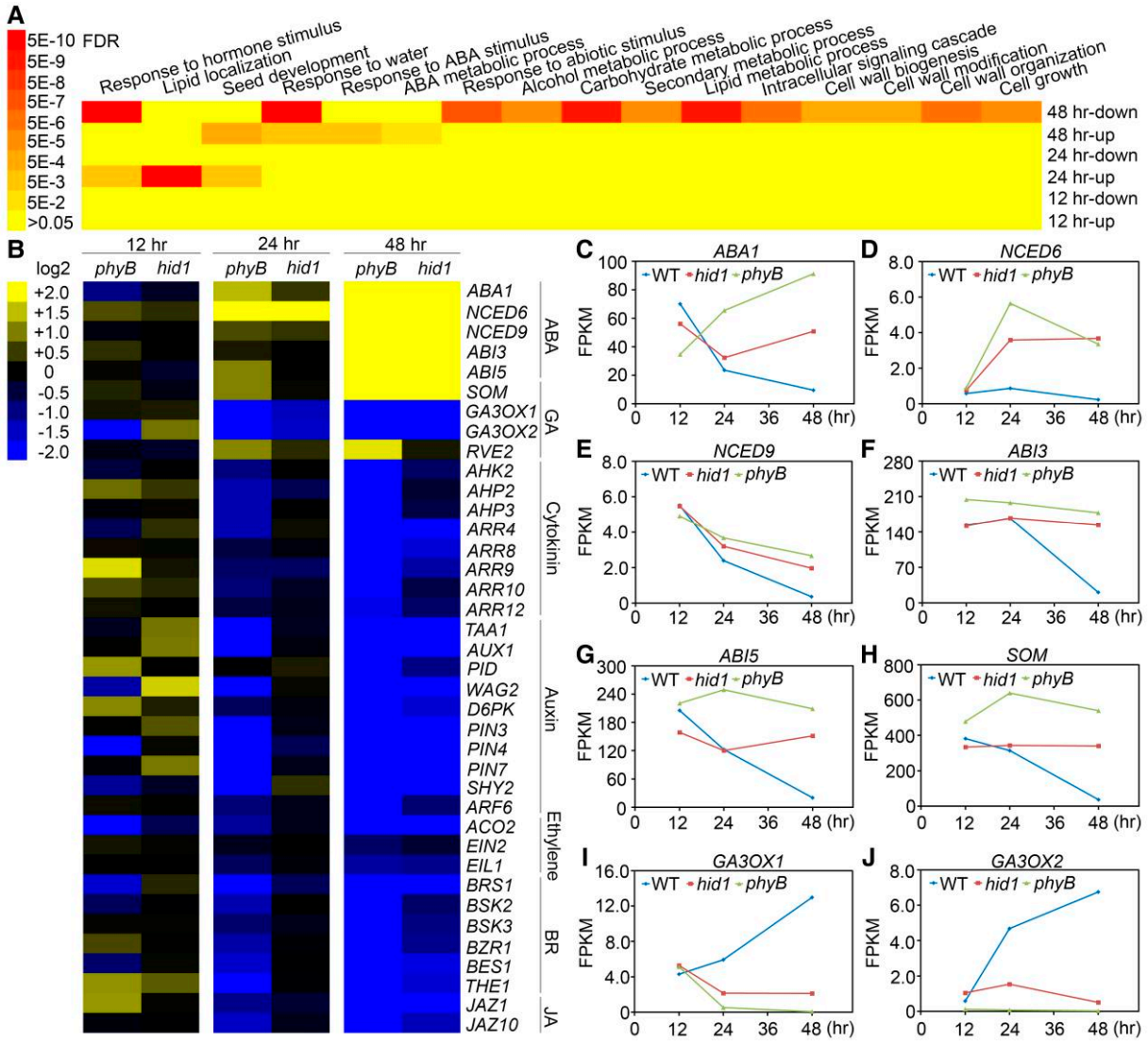

Figure 4 *HID1* promotes phyB-dependent seed germination by regulating the expression of metabolic and signaling genes related to ABA and GA. A, GO term analysis of differentially expressed genes in *hid1* mutants in comparison with WT following 12, 24, and 48 h DAL. "up" or "down" indicates upregulated or downregulated genes, respectively, in *hid1* mutants in comparison with WT. B, Cluster analysis of *hid1*- and *phyB*-regulated genes. The scale bar shows the log2 transformation of the ratio. C–J, FPKM (fragments per kilobase per million mapped reads) values (from the RNA-seq data) of the indicated genes in WT, *hid1*, and *phyB* following 12, 24, and 48 h DAL under phyB-on conditions.

also generated *hid1 phyB* double mutants. From the seed germination analysis, we found that the *hid1 phyB* double-mutant failed to germinate under phyB-on conditions, which phenocopied the *phyB* single mutant (Supplemental Figure S5, A and B). RT-qPCR demonstrated that the mRNA levels of selected genes involved in ABA biosynthesis and signaling were significantly upregulated in the *hid1* line compared to the WT. The expression levels of these genes in the *phyB* and *hid1 phyB* double mutants were ~20-fold greater than in the WT (Supplemental Figure S5C). By contrast, the expression levels of GA biosynthesis genes were downregulated in the *hid1*, *phyB*, and *hid1 phyB* double-mutant lines (Supplemental Figure S5D). Taken together, these results suggest that *HID1* acts genetically downstream of *phyB* to mediate transcriptome changes that promote seed germination.

HID1 promotes phyB-dependent seed germination predominantly by suppressing ABA biosynthesis

To further explore the mechanism by which *HID1* regulates phyB-dependent seed germination, we performed forward genetic screening to identify key downstream components of the phyB-*HID1* pathway. The screening process identified four independent recessive alleles in the M2 population of the ethylmethanesulfonate (EMS)-mutagenized *hid1* mutant, and mutations in each of these alleles completely suppressed the delayed germination phenotype of *hid1* under phyB-on conditions (Figure 5, A and B). Map-based cloning

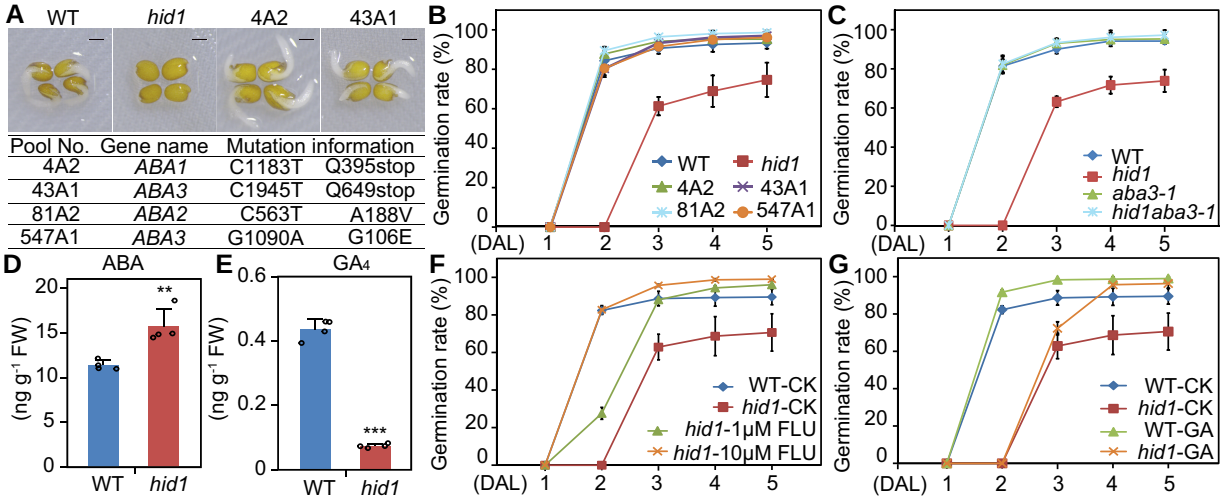

Figure 5 *HID1* promotes phyB-dependent seed germination by repressing ABA biosynthesis. A, Representative images of WT, *hid1*, and two genetic suppressor lines of *hid1* (4A2 and 43A1) following 48 h DAL under phyB-on conditions. Scale bar, 1 mm. The table underneath shows mutational information for the *HID1* suppressor genes. B, Germination rates of WT, *hid1*, and four genetic suppressor lines of *hid1* (4A2, 43A1, 81A2, and 547A1) following 48 h DAL under phyB-on conditions. Germination frequencies were recorded every 24 h after light treatment. Mean ± SD, $n = 3$. C, Germination rates of WT, *hid1*, *aba3-1*, and the *hid1 aba3-1* double-mutant following 48 h DAL under phyB-on conditions. Mean ± SD, $n = 3$. D and E, Quantitation of endogenous ABA (D) and GA_4 (E) levels in WT and *hid1* mutant seeds following 48 h DAL under phyB-on conditions. FW, fresh weight. Mean ± SD, $n = 4$. ** $P \leq 0.01$, *** $P \leq 0.001$ (two-tailed Student's *t*-test). F and G, Germination rates of WT and *hid1* mutant seeds exposed to different chemical treatments. CK, no chemical treatment; FLU, Fluridone; GA, GA_3. Mean ± SD, $n = 3$.

enabled the identification of three ABA biosynthesis genes, *ABA1*, *ABA2*, and *ABA3*, as candidate suppressors of *HID1* (Figure 5A). The mutants 4A2 and 43A1 contained a single C to T nucleotide change in the coding region of *ABA1* and *ABA3*, respectively, resulting in an amino acid change to a stop codon. Mutants 81A2 and 547A1 contained a nucleotide change in the coding region of *ABA2* and *ABA3*, resulting in a missense mutation in their amino acid sequence (Figure 5A). We generated a *hid1 aba3-1* double-mutant to validate the genetic relationship between *HID1* and *ABA3*. From the phenotypic analysis, we found that the germination rates of *aba3* and *hid1 aba3* were similar to that of the WT line (Figure 5C), indicating that *ABA3* acts downstream of *HID1* during phyB-dependent seed germination. Next, we examined the endogenous levels of ABA and GA in imbibed WT and *hid1* seeds following 48 h DAL under phyB-on conditions and found that ABA levels in the *hid1* seeds were significantly higher than those in the WT seeds (Figure 5D). By contrast, the content of GA_4, the major bioactive GA, was much lower in the *hid1* seeds than in the WT seeds, while the concentrations of precursor GA_9 and deactivated GA_{51} were increased in the *hid1* seeds than in the WT seeds (Figure 5E; and Supplemental Figure S6). These results indicate that *HID1* promotes low levels of ABA and high levels of GA following 48 h DAL.

Subsequently, to determine whether the ABA level in the *hid1* mutant line is the primary contributor to *HID1*-mediated seed germination, we treated WT and *hid1* mutant seeds with the ABA synthesis inhibitor fluridone (FLU). Exposure to 10 μM FLU fully rescued the delayed germination phenotype of the *hid1* mutants to that of the WT (Figure 5F). In addition, the delayed germination phenotype of the *hid1* mutants was only slightly rescued following the application of 5 μM bioactive GA_3 to the MS media (Figure 5G). Collectively, these results demonstrate that activation of the phyB-*HID1* axis promotes seed germination following 48 h DAL predominantly by repressing ABA biosynthesis.

HID1 binds to *NCED9* chromatin and inhibits it transcription

The results of our previous study suggested that *HID1* binds chromatin and regulates transcription (Wang et al., 2014a, 2014b). To gain further insight into the molecular mechanisms underlying *HID1* function, we investigated the genomic binding sites of *HID1* using chromatin isolation by RNA purification (ChIRP) and subsequent high-throughput sequencing (Chu et al., 2011). We compared two chemical crosslinking strategies for fixing *HID1*:DNA:protein interactions with formaldehyde and glutaraldehyde. Using probes complementary to *HID1* RNA, 15% and 12% of the total *HID1* RNA were specifically retrieved by 1% formaldehyde and 1% glutaraldehyde crosslinking, respectively (Figure 6A). Strong *HID1* peaks were identified using each of the crosslinkers, suggesting that the *HID1* ChIRP-seq procedure obtained a reliable signal.

In total, 396 genes that gave peaks in the ChIRP-seq experiments with both crosslinkers were considered *HID1*-bound gene candidates (Supplemental Data Set 2). Among these genes, 55 were upregulated and 76 were downregulated in the *hid1*

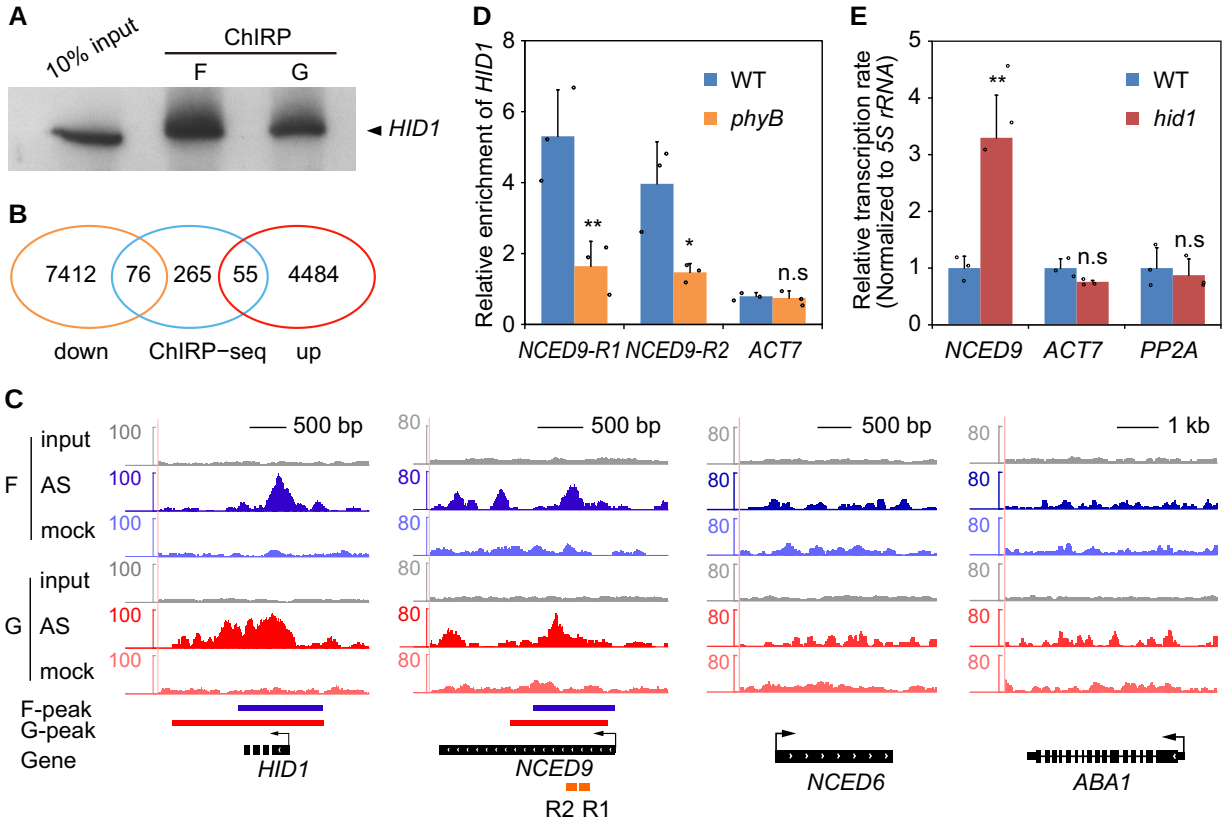

Figure 6 *HID1* associates with the *NCED9* locus and represses its transcription. A, RNA gel blots of *HID1*. *F* indicates 1% (v/v) formaldehyde crosslinking, and *G* indicates 1% (v/v) glutaraldehyde crosslinking. B, Venn diagram of *HID1*-regulated and *HID1*-bound genes identified by ChIRP-seq. The overlapping ChIRP peaks were identified by both formaldehyde- and glutaraldehyde-crosslinked ChIRP-seq. C, *HID1* association with the *NCED9* locus by ChIRP-seq. F indicates formaldehyde crosslinking and G indicates glutaraldehyde crosslinking. D, ChIRP-qPCR showing the differences in *HID1* occupancy on chromatin at *NCED9* in WT and *phyB*. Mean ± SD, $n = 3$. n.s, no significance. * $P \leq 0.05$, ** $P \leq 0.01$ (two-tailed Student's *t*-test). E, The nascent RNA levels of *NCED9* in WT and *hid1* seeds following 48 h DAL under phyB-on conditions were determined by the nuclear run-on assay. 5S rRNA was used as an internal control. Mean ± SD, $n = 4$. n.s, no significance. ** $P \leq 0.01$ (two-tailed Student's *t*-test).

mutants at 48 h under phyB-on conditions (Figure 6B). Interestingly, we found strong peaks at the genomic locus of *NCED9*, a key enzyme in ABA biosynthesis (Figure 6C). Subsequent ChIRP-qPCR experiments confirmed the binding of *HID1* on the chromatin of the *NCED9* gene body (Figure 6D). Notably, the occupancy of *HID1* at *NCED9* was greatly reduced in the *phyB* mutants, suggesting that phyB is required for the binding of *HID1* at *NCED9* during seed germination (Figure 6D). We next examined the transcription rate of *NCED9* by performing nuclear run-on (NRO) assays in WT and *hid1* mutant lines. Loss of *HID1* significantly increased the *NCED9* transcription rate, while the transcription rates of *ACT7* and *PP2A* were unaffected (Figure 6E), suggesting that *HID1* inhibits *NCED9* expression at the transcriptional level.

HID1 inhibits the enrichment of H3K4me3 on its repressed target genes

LncRNAs have been shown to be key regulators of histone modification on chromatin at specific genomic loci to modulate gene expression *in cis* and/or *in trans* (Statello et al., 2021). To assess whether *HID1* mediates changes in histone modification on its target genes during phyB-dependent seed germination, we examined the genomic profiles of the active gene expression mark H3K4me3 and the repressive gene expression mark H3K27me3 in imbibed WT and *hid1* seeds following 48 h DAL under phyB-on conditions. To this end, antibodies against H3K4me3 and H3K27me3 were used in chromatin-immunoprecipitation (ChIP)-seq experiments (Supplemental Data Sets 3 and 4). The 131 differentially expressed and *HID1*-bound genes were selected for subsequent analysis. In *hid1* (*hid1*/WT), a change in the H3K4me3 level (R = 0.77), but not in the H3K27me3 level (R = 0.05), was positively correlated with changes in the expression of the 131 *HID1* target genes (Figure 7, A and B). These results suggest that *HID1*-directed transcriptional changes may be coupled to H3K4me3 changes. We next created a meta-plot of H3K4me3 modification on *HID1* target genes. The density of H3K4me3 was markedly higher on the 5′-end of *HID1*-repressed target genes in *hid1* compared with WT, while H3K4me3 density was reduced on *HID1*-activated genes (Figure 7C). These results indicate that *HID1* may modulate H3K4me3 occupancy and regulate target gene expression.

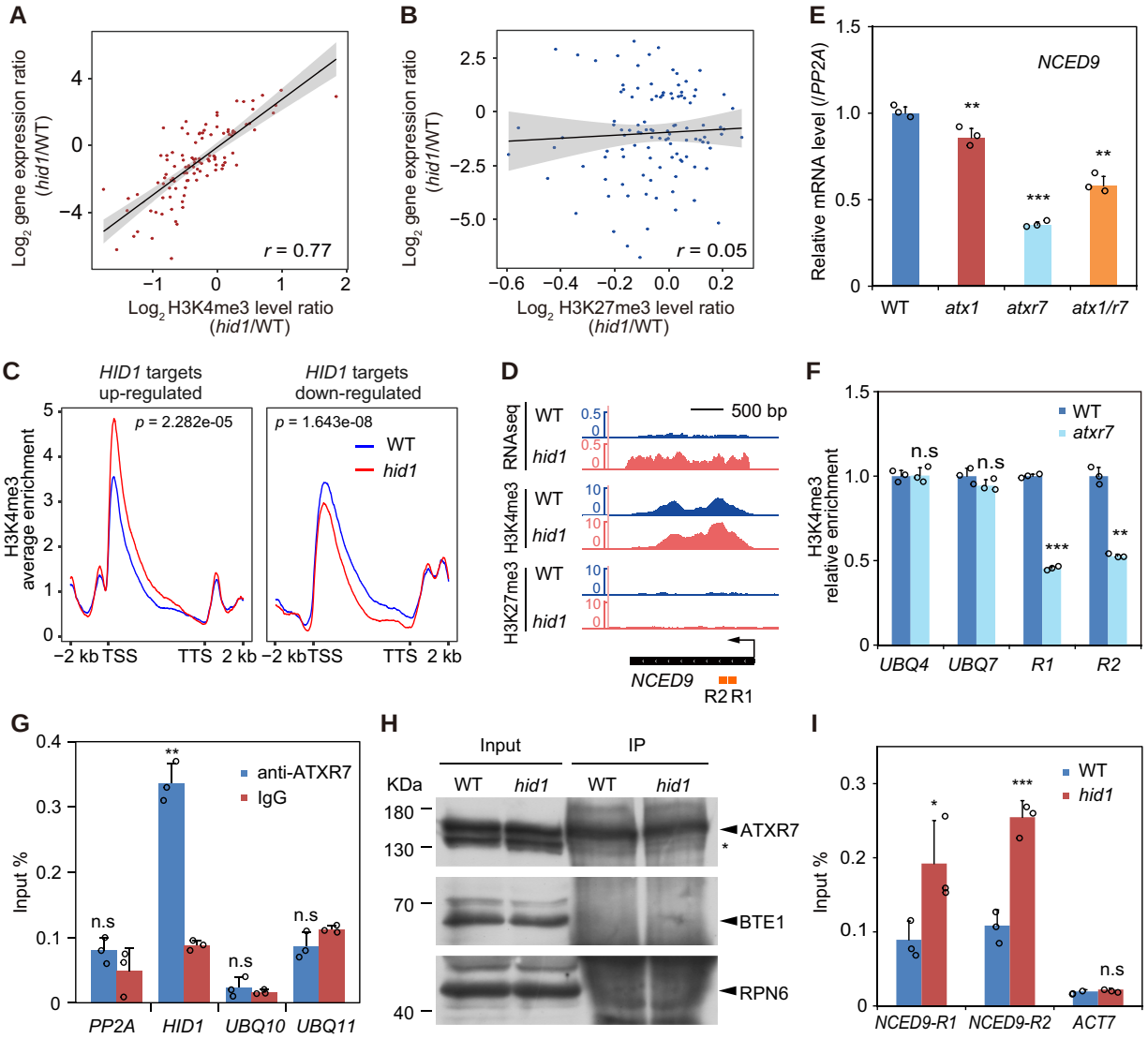

Figure 7 *HID1* antagonizes the accumulation of H3K4me3 and ATXR7 at the *NCED9* locus. The correlation scatterplots show the log2 fold change values of the mRNA and H3K4me3 levels (A) and the H3K27me3 levels (B) in *hid1* as compared with WT at 48 h under phyB-on conditions. r, Pearson's correlation coefficient. C, Meta-plots of the ChIP-seq signal of H3K4me3 for *hid1*-upregulated genes and *hid1*-downregulated genes in WT (blue curve) and *hid1* (red curve). *P* value as indicated by the Wilcoxon rank-sum test. D, Integrative Genomics Viewer (IGV) screenshots of the RNA-seq, H3K4me3 ChIP-seq, and H3K27me3 ChIP-seq signals at *NCED9*. The gene model is shown at the bottom by the black bar. The arrow indicates the direction of transcription. E, RT-qPCR showing the mRNA levels of *NCED9* in WT, *atx1*, *atxr7*, and *atx1 atxr7* seeds following 48 h DAL under phyB-on conditions. Mean ± SD, $n = 3$. *** $P \leq 0.001$ (two-tailed Student's *t*-test). F, ChIP-qPCR showing the relative enrichment of H3K4me3 on the indicated genes in WT and *atxr7*. Mean ± SD, $n = 3$. n.s, no significance. ** $P \leq 0.01$, *** $P \leq 0.001$ (two-tailed Student's *t*-test). *UBQ4* and *UBQ7* were used as controls. G, RIP-qPCR showing the association between ATXR7 and *HID1*. Mean ± SD, $n = 3$. n.s, no significance. ** $P \leq 0.01$ (two-tailed Student's *t*-test). H, Immunoblots showing the protein expression levels of ATXR7 in the input and immunoprecipitates (IP) from WT and *hid1*. BTE1 and RPN6 were used as the loading controls. I, ChIP-qPCR showing the enrichment of ATXR7 at the indicated DNA regions of *NCED9* in WT and *hid1*. *ACT7* was used as the control. Mean ± SD, $n = 3$. n.s, no significance. *** $P \leq 0.001$ (two-tailed Student's *t*-test).

HID1 disrupts the binding of ATXR7 at *NCED9*

In Arabidopsis, H3K4me3 is catalyzed by methyltransferases embedded in conserved COMPASS-like complexes (Hu and Du, 2022). Seven methyltransferases catalyze H3K4 methylation in Arabidopsis, including Trithorax group proteins ARABIDOPSIS TRITHORAX 1–5 (ATX1–5) and ATX-related (ATXR) proteins 3 and 7 (Hu and Du, 2022). Among these methyltransferases, ATX1 mediates the establishment of H3K4me3 and activates the expression of genes regulating plant meristem homeostasis, flowering, and ABA-dependent stress responses (He et al., 2021). ATXR7, an Arabidopsis homolog of yeast SET1, is also a methyltransferase for H3K4me3 (Tamada et al., 2009) and is known to play a role in seed dormancy (Liu et al., 2011). Recalling that the level of H3K4me3 at the *NCED9* locus was increased in the *hid1* mutant compared with WT (Figure 7D) and that *HID1* binding coincided with the H3K4me3 peak at the 5′-end of *NCED9*

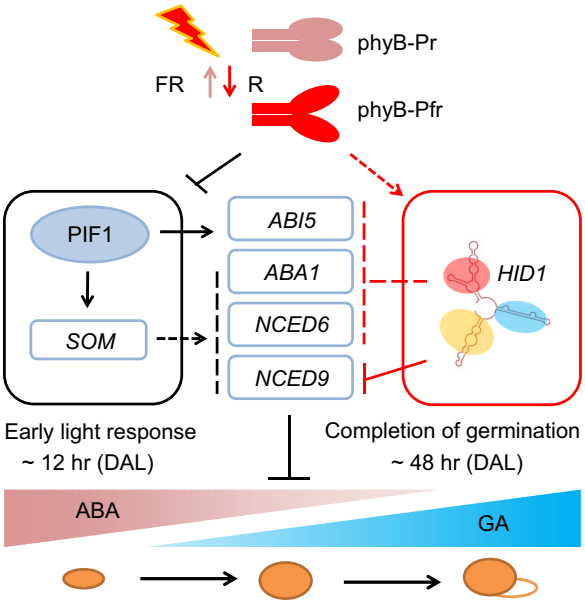

Figure 8 A simplified working model of phyB-dependent seed germination mediated by *HID1*. Previous studies have shown that upon activation by red light, the Pfr form of phyB mediates the rapid degradation of PIF1 as an early light response. This inhibits PIF1-induced transcription of ABA biosynthesis genes via a SOMNUS-dependent pathway. Following 48 h DAL, the expression of the noncoding RNA *HID1* in the radicles is significantly increased in a phyB-dependent manner. *HID1* directly and indirectly inhibits the expression of ABA biosynthesis genes to promote phyB-dependent seed germination. Solid arrows, direct positive regulation; Dashed arrows, indirect positive regulation; Solid bars, direct negative regulation; Dashed bars, indirect negative regulation.

(Figure 6C), we speculated that *HID1* mediates the transcriptional repression of *NCED9* by regulating H3K4me3 modification. We initially measured the expression of *NCED9* in *atx1* and *atxr7* single mutants and found that the mRNA level of *NCED9* was strongly downregulated in the *atxr7* mutant (more than two-fold) but only slightly reduced in *atx1* (Figure 7E). Moreover, the expression of *NCED9* in the *atx1 atxr7* double-mutant closely resembled that of the *atxr7* single mutant (Figure 7E). These results raised the possibility that *NCED9* is a direct target of ATXR7; therefore, we used the *atxr7* single mutant to determine whether ATXR7 is essential for H3K4me3 deposition at *NCED9*. We found that depletion of *ATXR7* resulted in a marked reduction in the H3K4me3 level at *NCED9*, but not at the control genes *UBQ4* and *UBQ7* (Figure 7F), suggesting that ATXR7 is required for H3K4me3 deposition and activation of *NCED9*.

We next examined whether *HID1* inhibits the enrichment of ATXR7 at *NCED9*. By generating an antibody against endogenous ATXR7 in Arabidopsis (Supplemental Figure 7), we assessed the interaction between *HID1* and ATXR7 in vivo by RNA immunoprecipitation (RIP) using total protein lysates extracted from imbibed WT seeds following 48 h DAL under phyB-on conditions. Our results showed that ATXR7 co-immunoprecipitated with *HID1* in vivo (Figure 7, G and H). To further determine the role of *HID1* in the targeting of *NCED9* by ATXR7, we compared the enrichment of ATXR7 at *NCED9* in the WT and *hid1* mutant lines. ChIP-qPCR data clearly demonstrated that the occupancy of ATXR7 on *NCED9* chromatin within ATXR7 peak regions was greatly enhanced in the *hid1* mutant compared with the WT, suggesting that *HID1* inhibits the binding of ATXR7 at *NCED9* (Figure 7I).

Discussion

Plants have evolved ingenious mechanisms to regulate seed germination. In general, from imbibition to radicle protrusion, it takes ~2 days for Arabidopsis seeds to germinate after perceiving a light signal via photoreceptors (Seo et al., 2009; Shi et al., 2013). A better understanding of how photoreceptors transduce external light signals into internal phytohormone signaling to induce genome-wide changes in transcription during seed germination will provide important insight into seed biology. In the present study, we explored the molecular framework underlying a transcriptional cascade through which phyB-promoted radicle accumulation of the ncRNA *HID1* inhibits ABA biosynthesis to promote seed germination during prolonged imbibition following 24 h DAL (Figure 8). It is likely that red light-activated phyB mediates short- and long-term effects to decrease the transcription of ABA biosynthesis genes. It is well accepted that for short-term effects, phyB promotes the degradation of PIF1 via the 26S proteosome. For long-term effects, at least in part, phyB promotes the reduction of ABA biosynthesis and signaling genes transcription via *HID1*. The results of this study demonstrate that activation of the phyB-*HID1* genetic axis promotes red light-initiated seed germination. Our work establishes a new link between phyB and ABA biosynthesis genes via *HID1*, revealing another layer of light-dependent regulation of seed germination mediated by noncoding RNA.

It has been reported that ABA content decreases rapidly in imbibed seeds. The decrease in ABA content at the beginning of seed imbibition is not dependent on light quality; however, the continuous decrease in ABA levels that occurs during prolonged imbibition (seeds imbibed for more than 24 h) is regulated by light (Seo et al., 2009). The manner by which light signaling regulates ABA biosynthesis and maintains the germination signal in imbibed seeds is unclear. Our genetic and transcriptomics analyses suggest that *HID1* acts downstream of phyB to regulate ABA biosynthesis (Figure 3; and Supplemental Figure S4). Forward genetic screening identified three ABA biosynthesis genes, *ABA1*, *ABA2*, and *ABA3*, as candidate targets of *HID1* suppression, suggesting that *HID1* inhibits the biosynthesis of ABA in imbibed seeds (Figure 5). Indeed, the ABA levels in the *hid1* mutants were higher than those in the WT line. ChIRP-seq and nuclear run-on experiments demonstrated that *HID1* directly binds to the chromatin of the ABA biosynthesis gene *NCED9* and inhibits its transcription. Hence, these results indicate that *HID1* inhibits ABA biosynthesis to promote seed germination

primarily by inhibiting the expression of ABA biosynthesis genes, both directly and indirectly. Interestingly, exogenous application of the ABA biosynthesis inhibitor FLU completely rescued the *hid1* mutant phenotype to that of the WT, yet the exogenous application of GA hardly improved the germination rate of *hid1* seeds (Figure 6). These results suggest that, although the ABA content in the imbibed seeds following 48 h DAL under phyB-on conditions was already low, modulation of ABA levels at this stage may have a stronger effect on seed germination in comparison with an increase in GA levels. Thus, the phyB-*HID1*-*ABA1*/*NCED6*/*NCED9* transcriptional cascade may play a regulatory role in the maintenance of the signal-promoting seed germination.

Previous studies have demonstrated the presence of a decision center in the embryonic radicle of dormant seeds, which plays an important role in the decision to germinate in diverse environments. In the radicle, the responses to ABA and GA occur in a distinct spatial configuration, with the ABA response enriched in the tip of the radicle and the GA response enriched in the hypocotyl of the embryo, including the vascular tissue (Oh et al., 2006; Topham et al., 2017). The pronounced expression of *HID1* in radicle cells following 48 h DAL can be related to its function in modulating ABA biosynthesis. Investigation into the manner by which phyB mediates the spatiotemporal expression of *HID1* is underway. Photoactivated phyB may promote the expression and activity of *HID1* during seed germination as a long-term effect. We speculate that there may exist a general repression mechanism or low positive effect immediately after the activation of phyB by red light in order to maintain *HID1* accumulation at a certain level in the radicle following 12 and 24 h DAL. After 24 h DAL, the significant increase in *HID1* expression in the radicle may be achieved by the gradual activation or deactivation of positive or negative regulators of *HID1* transcription, respectively. Future studies are required to delineate the manner by which phyB precisely regulates the expression of *HID1* in the decision center of the radicle.

As a large transcript reservoir, chromatin-associated lncRNAs can contribute to transcriptional regulation *in cis* or *in trans* by interacting with chromatin modifiers, mediating the recruitment or decoying of chromatin modifiers at specific genomic loci to modulate transcription (Long et al., 2017; Statello et al., 2021). Several research works in plants have revealed that chromatin-associated lncRNAs can regulate gene transcription by modulating histone H3K4me3 modification. For instance, *COLDAIR* (Liu et al., 2020) and *MAS* (Zhao et al., 2018) in Arabidopsis, as well as *LAIR* (Wang et al., 2018a, 2018b) in rice, mediate the recruitment of H3K4me3 to activate gene expression and affect Arabidopsis flowering and rice yield. However, the manner by which lncRNAs function *in trans* to regulate H3K4me3 and gene transcription is poorly understood. In this study, we found that ectopic expression of *HID1* in the *hid1* mutant rescued the delayed seed germination phenotype under phyB-on conditions, suggesting that *HID1* functions *in trans* to regulate gene transcription during seed germination. We further explored the repressive role of *HID1* on H3K4me3 deposition and gene transcription at *NCED9 in trans*. We demonstrated that *HID1* inhibits the occupancy of ATXR7, a methyltransferase for H3K4me3, at *NCED9* and reduces the levels of H3K4me3 modification and *NCED9* transcription. Our results suggest a likely role for *HID1* as a molecular decoy that interfaces with epigenetic machinery to regulate the chromatin environment at specific gene loci during the completion of seed germination. It is also possible that *HID1* may function by affecting the interactions among components in the ATXR7-containing methyltransferase complexes and/or impairing ATXR7 H3K4 methyltransferase activity. The mechanisms by which chromatin-associated lncRNAs, including *HID1*, interact with ATXR7 in terrestrial plants to regulate H3K4me3 levels and gene transcription merit further investigation.

Our series of work has identified *HID1*, a plant-specific and conserved noncoding RNA, as an essential player in the control of multiple light-dependent biological processes including seed germination, seedling greening during de-etiolation, and photomorphogenesis. Interestingly, in all scenarios, *HID1* acts as a negative regulator on chromatin to repress the transcription of different target genes *in trans* beyond Polycomb Repressive Complex 2 (PRC2)-mediated gene repression. We speculate that *HID1* may modulate chromatin dynamics at specific genomic loci through various mechanisms, including, but not limited to, interfacing with epigenetic machinery, transcription factors, and transcriptional co-regulators in a light-dependent manner. Moreover, future studies should investigate ways in which the *HID1*–chromatin interaction can be modulated to regulate the transcription of specific target genes in light-mediated plant growth and development.

Materials and methods

Plant materials and growth conditions

The ecotype of all WT *Arabidopsis thaliana* used in this study was Columbia-0 (Col-0). The *hid1* mutant (SALK_017318), the transgenic lines used in this study (*HID1*/*hid1*#2, *HID1*/*hid1* #4, *mut1*/*hid1*#6, *mut2*/*hid1*#5, *dSL2*/*hid1*, *dSL4*/*hid1*, *OsHID1*/*hid1*#2, *OsHID1*/*hid1*#5, and *35S:HID1*/WT), and *phyB-9* have been reported previously (Wang et al., 2014a, 2014b). *35S:HID1*/phyB was obtained by crossing *35S:HID1*/WT *with phyB-9*. *aba3-1* (CS157), *atx1* (SALK_149002), and *atxr7* (SALK_149692) were ordered from the Arabidopsis Biological Resource Center. *hid1 aba3-1* double mutants were obtained by crossing *hid1* with *aba3-1*, and *atx1 atxr7* double mutants were obtained by crossing *atx1* with *atxr7*. Arabidopsis seed sterilization, stratification, and standard seedling growth experiments were performed as previously described (Zhu et al., 2008). For seed germination-related experiments, all plants were grown side-by-side, and the seeds were harvested on the same day. The seeds were dried at room temperature for 2–6 months prior to conducting experiments, unless otherwise stated. Before performing any

experiments, the germination rates of all the seeds were checked to ensure almost 100% germination at Day 3 after planting under continuous WL.

Germination assays

Including sterilization and plating, seeds were exposed to WL (50 μmol m^{-2} s^{-1}) for 1 h. Under phyB-off conditions, seeds were exposed to far-red light (5 μmol m^{-2} s^{-1}) for 5 min to inactivate phyB. Under phyB-on conditions, seeds were then irradiated with red light (20 μmol m^{-2} s^{-1}) for 5 min to activate phyB. Under phyA-on conditions, seeds were irradiated with far-red light (FR) (5 μmol m^{-2} s^{-1}) for 4 h, to activate phyA at 48 h and then incubated in the dark for 3 days. Under WL conditions, seeds were exposed to continuous WL for 1 h, stratified at 4°C for 3 days in the dark before being planted, and then incubated under continuous WL for a further 5 days. Germination rates were recorded every 24 h after planting. The seeds were then incubated in the dark for the indicated time, and the germination rates were determined in a dark room. At least 120 seeds were used for each experimental treatment, and three biological replicates were performed for each statistical analysis.

Plasmid construction and generation of transgenic plants

To generate the *pHID1:GUS* construct, the 1.5 kb upstream regulatory sequence of *HID1* was cloned into the Gateway vector pDONR221 (Invitrogen) using BP Clonase and transferred into the binary vector pBGWFS7 by the LR reaction (Invitrogen). To generate the *pHID1:Broccoli-HID1* construct, the *Broccoli* sequence was inserted into *HID1* by PCR-based mutagenesis using a *pHID1:HID1* plasmid as the template and then cloned into the BamHI site of pCAMBIA1300 . To generate the *35S:mCherry-SV40-NLS* construct, the SV40-NLS sequence was fused with the mCherry coding sequence at the 3′end by PCR and then cloned into the BamHI/XbaI sites of pCAMBIA3300.

Agrobacterium tumefaciens strain GV3101 was used to transform Arabidopsis plants of the indicated backgrounds using the floral dip method (Clough and Bent, 1998). All transgenic plants were obtained by antibiotic selection and verified by immunoblotting and/or RNA gel blotting. *pHID1:GUS/phyB* was obtained by crossing *pHID1:GUS*/WT with *phyB-9*.

All cloning primers are listed in Supplemental Table S1.

GUS staining

GUS staining was performed as previously reported (Zhang et al., 2008a, 2008b).

In situ hybridization

In situ hybridization was performed as previously described (Wu and Wagner, 2012). Digoxigenin (DIG)-labeled *HID1* antisense and sense probes were transcribed using the AmpliScribe T7-Flash Transcription Kit (Illumina).

RNA gel blotting

RNA gel blotting was performed as previously reported (Liu et al., 2013). The sequence used to probe *HID1* is listed in Supplemental Table S1.

RNA imaging

Plant materials were incubated in RNA Imaging Buffer [20 mM HEPES-KOH (pH 7.5), 0.3 mM $MgCl_2$, 100 mM KCl, 200 μM DFHBI-1 T] for 5 min at room temperature. Images were taken using a Zeiss LSM800 confocal microscope. For the *Broccoli* channel, the excitation wavelength was 488 nm, and the emission wavelength range was 490–520 nm. For the mCherry channel, the excitation wavelength was 561 nm, and the emission wavelength range was 600–670 nm.

Quantitative RT-PCR and RNA-seq

Total RNA was isolated using the Spectrum Plant Total RNA Kit (STRN50, Sigma). For quantitative RT-PCR (RT-qPCR), 1 μg total RNA was used to synthesize cDNA with SSRIII transcriptase (Invitrogen). Real-time PCR was performed using the SYBR Premix Ex Taq Kit (Takara) on a 7500 Fast Real-Time PCR Amplifier (Applied Biosystems). *ACTIN7*, *5S rRNA*, and *PP2A* were used as the internal controls as indicated in different figures. The primers used for RT-qPCR are listed in Supplemental Table S1.

For RNA-seq, three biological replicates for each sample were used for library generation. Poly(A) RNA from 1 μg total RNA was used to generate each cDNA library according to the TruSeq RNA Sample Prep Kit (Illumina) protocol. All libraries were sequenced on a HiSeq 2500 System (Illumina) with 150 bp paired-end reads. RNA-seq reads were mapped to TAIR10 using HISAT2 (version 2.1.0). Differentially expressed genes were defined as those that differed by more than 1.5-fold with a false discovery rate <0.01 using the edgeR software (version 2.0.0) (Robinson et al., 2010).

ChIP and ChIP-seq library preparation

ChIP was carried out as outlined previously, with minor modifications (Gendrel et al., 2005). Briefly, 0.3 g seedlings grown under phyB-on conditions for 48 h were collected, crosslinked with 1% formaldehyde for 20 min under a vacuum, and ground into a fine powder in liquid nitrogen. Chromatin was isolated and sheared into fragments (200–500 bp) by sonication and incubated with antibody-bound Sera-Mag SpeedBeads Protein A/G Magnetic Particles (17152104010150, GE Healthcare) overnight at 4°C. Precipitated DNA was reverse-crosslinked, digested with RNase A and Proteinase K, and purified using the ChIP DNA Clean & Concentrator Kit (D5205, Zymo Research) according to the manufacturer's instructions. Three biological replicates for each sample were subjected to ChIP-seq. All ChIP-seq libraries were generated with the NEBNext® Ultra II DNA Library Prep Kit for Illumina® (E7645S, NEB) according to the manufacturer's instructions. All libraries were sequenced on a HiSeq2500 System with 150 bp paired-end reads. The antibodies used for ChIP were anti-H3K4me3 (04-745, Millipore, 1:200 dilution),

anti-H3K27me3 (07-449, Millipore, 1:100 dilution), and anti-ATXR7 (raised in rabbit using the synthetic peptide LIRDGENKLRPITLC as the antigen, Beijing Protein Innovation, 1:200 dilution). The primers used for ChIP-qPCR are listed in Supplemental Table S1.

ChIP-seq data analysis

For all ChIP-seq data sets, reads were aligned to the Arabidopsis genome (TAIR10) (Lamesch et al., 2012) using bowtie2 (version 2.3.4) (Langmead and Salzberg, 2012) with default parameters. Only unique alignments of high mapping quality (MAPQ > 30) were retained by SAMtools (Li et al., 2009). The alignments were converted to bigWig files using the bamCoverage tool from deepTools2 (version 3.1.3) (Ramirez et al., 2016) with parameters "–binSize 5 –normalizeUsing CPM". Meta-gene-averaged ChIP-seq profiles were generated in deepTools2 using the computeMatrix tool and plotted with the ggplot2 (version 3.2.1) package.

Suppressor screening and gene mapping

The *hid1* mutant seeds were soaked in water overnight, treated with 0.4% (v/v) EMS solution for 8 h, washed extensively with sterile water, and dried. Plants (5,000 M1) were grown in groups of 1,000. M2 plants were screened for the WT phenotype as suppressor candidates. Four independent M3 candidate suppressors that were no longer segregated for the *hid1* phenotype were identified and crossed with Landsberg *erecta* to generate the mapping population. Rough mapping and fine mapping were carried out as previously described (Qu and Qin, 2014). The markers used for map-based cloning were designed according to the Monsanto Arabidopsis polymorphism and Landsberg sequence collections.

Quantitation of endogenous ABA and GA levels

For each genotype, 0.3 g seeds grown under phyB-on conditions for 48 h were collected, frozen in liquid nitrogen, and ground into a fine powder in a dark room. Endogenous ABA and GA were purified and measured as previously described (Jiang et al., 2021). Statistical analysis was performed on four experiments using individual batches of seeds.

Immunoprecipitation and immunoblotting

For immunoprecipitation (IP) assays, seed samples (0.5 g) were frozen in liquid nitrogen, ground into a powder, and placed in lysis buffer (50 mM Tris-HCl [pH 8.0], 150 mM NaCl, 1 mM EDTA, 10% (v/v) glycerol, 0.1% (v/v) Tween®20, 1 mM PMSF, and 1× protease inhibitors). Samples were centrifuged at 16,000 × *g* for 10 min, and the total protein concentration of the supernatants was determined by the Bradford method. A 50 μg aliquot of total protein was taken as input, and 500 μg total protein was incubated with 5 μl purified anti-ATXR7 antibody in 500 μl lysis buffer for 4 h at 4°C. Subsequently, 20 μl well-washed Protein A/G magnetic beads (17152104010150, GE Healthcare) were added to each sample, and the tube was rotated for 2 h at 4°C. The beads were washed three times with lysis buffer, and proteins were eluted from the beads by boiling in 1× SDS loading buffer. Immunoblotting was performed as previously reported (Zhu et al., 2008). The anti-BTE1 (1:1000 dilution) and anti-RPN6 (1:2000 dilution) antibodies used in this study have been reported previously (Wang et al., 2022).

Chromatin isolation by RNA purification

ChIRP was performed as previously described, with some modifications (Chu et al., 2011). A total of 0.3 g seeds were used for each assay. The materials were fixed using two methods in the dark room. For reversible chemical crosslinking, fixation was performed with 1% (v/v) formaldehyde in PBS at room temperature for 20 min under a vacuum. For nonreversible crosslinking, fixation was performed with 1% (v/v) glutaraldehyde in PBS at room temperature for 20 min under a vacuum. For both crosslinking methods, the reactions were quenched with glycine (0.125 M final concentration) for 5 min under a vacuum. Antisense DNA probes were designed against the full-length *HID1* sequence and biotinylated at the 3′ end (Invitrogen). Unlabeled probes were used as a control. DNA was purified using the ChIP DNA Clean & Concentrator Kit (D5205, Zymo Research) according to the manufacturer's instructions, and purified DNA was subjected to high-throughput sequencing. All ChIRP-seq libraries were generated using the NEBNext® Ultra II DNA Library Prep Kit for Illumina (E7645S, NEB) according to the manufacturer's instructions. All libraries were sequenced on a HiSeq 2500 System with 150 bp paired-end reads. The primers used for ChIRP-qPCR are listed in Supplemental Table S1.

ChIRP-seq data analysis

Raw ChIRP sequence reads were mapped to the TAIR10 genome assembly (Lamesch et al., 2012) of Arabidopsis via bowtie2 (version 2.1.0) (Langmead and Salzberg, 2012) with default parameters. Only uniquely mapped reads of high MAPQ > 30 were retained for further analysis. Peak calling was performed using MACS (version 1.4.2) (Zhang et al., 2008a, 2008b) with the following parameters: –keep-dup 1 –gsize 1.2e8 –*P*value 1e5 –keep-dup = auto –to-large –nomodel –shiftsize 100. TAIR10 genome release was used for genomic region annotation of mapped ChIRP peaks. We defined ChIRP-associated genes as a ChIRP peak located in its gene body, 1500 bp upstream, or 500 bp downstream. Multiple gene-localized sites were retained for further verification.

Nuclear run-on assay

The nuclear run-on assay was performed as previously described (Zhu et al., 2016). A total of 0.3 g seeds were used for each assay. Four independent biological replicates were performed and analyzed. 5S *r*RNA was used as the internal control. The primers used for the nuclear run-on assay are listed in Supplemental Table S1.

RNA immunoprecipitation

RIP was performed as previously described (Wierzbicki et al., 2008). A total of 0.3 g seeds were used for each assay. Three independent biological replicates were performed and

analyzed. For immunoblotting, proteins were eluted from the beads by boiling in 1× SDS loading buffer. The antibodies used in this assay were ani-ATXR7 (raised in rabbit using the synthetic peptide LIRDGENKLRPITLC as the antigen, Beijing Protein Innovation, 1:200 dilution) and Rabbit IgG (PP64, Millipore, 1:200 dilution). The primers used for RIP are listed in Supplemental Table S1.

Statistical analysis

The germination rates, all of the RT-qPCR, ChIP-qPCR, ChIRP-qPCR, RIP-qPCR results, and endogenous ABA and GA levels obtained in this study are presented as means ± standard deviation (SD). The numbers of biological replicates in each experiment are noted in the figure legends. Statistical analysis was performed by a two-tailed Student's *t*-test. Wilcoxon rank-sum tests for the ChIP-seq signal of H3K4me3 levels in each sample were performed using R (https://www.R-project.org/). Details about the statistical analysis are provided in Supplemental Data Set 5.

Accession numbers

Accession numbers obtained from the Arabidopsis Information Resource (TAIR) for the genes mentioned in this article are as follows: *HID1*, AT2G35747; *PHYB*, AT2G18790; *ABA1*, AT5G67030; *NCED6*, AT3G24220; *NCED9*, AT1G78390; *ABI3*, AT3G24650; *ABI5*, AT2G36270; *SOM*, AT1G03790; *GA3OX1*, AT1G15550; *GA3OX2*, AT1G80340; *RVE2*, AT5G37260; *AHK2*, AT5G35750; *AHP2*, AT3G29350; *AHP3*, AT5G39340; *ARR4*, AT1G10470; *ARR8*, AT2G41310; *ARR9*, AT3G57040; *ARR10*, AT4G31920; *ARR12*, AT2G25180; *TAA1*, AT1G70560; *AUX1*, AT2G38120; *PID*, AT2G34650; *WAG2*, AT3G14370; *D6PK*, AT5G55910; *PIN3*, AT1G70940; *PIN4*, AT2G01420; *PIN7*, AT1G23080; *SHY2*, AT1G04240; *ARF6*, AT1G30330; *ACO2*, AT1G62380; *EIN2*, AT5G03280; *EIL1*, AT2G27050; *BRS1*, AT4G30610; *BSK2*, AT5G46570; *BSK3*, AT4G00710; *BZR1*, AT1G75080; *BES1*, AT1G19350; *THE1*, AT5G54380; *JAZ1*, AT1G19180; *JAZ10*, AT5G13220; *PIF1*, AT2G20180; *ACT7*, AT5G09810; *PP2A*, AT1G13320; *CYP707A2*, AT2G29090; *RGA*, AT2G01570; *RGL2*, AT3G03450; *EXP8*, AT2G40610; *EXP10*, AT1G26770; *ATX1*, AT2G31650; *ATXR7*, AT5G42400; *UBQ4*, AT5G20620; *UBQ7*, AT2G35635; *UBQ10*, AT4G05320; *UBQ11*, AT4G05050; *BTE1*, AT2G40630; *RPN6*, AT1G29150.

Data availability

RNA-seq, ChIP-seq, and ChIRP-seq data sets generated in this study have been deposited in the Gene Expression Omnibus (GEO) under accession GSE195748. All other study data are included in the article and/or supporting information.

Supplemental data

Supplemental Figure S1. ncRNA hid1 mutant seeds show a delayed germination phenotype under white light and phyA-on conditions.

Supplemental Figure S2. Broccoli-HID1 is biologically functional.

Supplemental Figure S3. phyB and PIF1, but not HID1, co-regulate the expression levels of a set of genes following 12 h DAL under phyB-on conditions.

Supplemental Figure S4. Expression patterns of genes involved in phytohormone signaling, cell wall loosening, water transport, and oil body formation over time during phyB-dependent seed germination.

Supplemental Figure S5. HID1 and phyB co-regulate metabolic and signaling genes related to ABA and GA.

Supplemental Figure S6. HID1 is essential for GA homeostasis following 48 h DAL under phyB-on conditions.

Supplemental Figure S7. Specificity test of the Anit-ATXR7 antibody in Arabidopsis.

Supplemental Figure S8. Unprocessed immunoblots in this study.

Supplemental Table S1. Primers and probes used in this study.

Supplemental Data Set 1. Differentially expressed genes in the WT and mutants over time during phyB-dependent seed germination obtained from the RNA-seq analysis.

Supplemental Data Set 2. The list of *HID1*-bound genes identified by ChIRP-seq.

Supplemental Data Set 3. Gene lists summarizing ChIP-seq analysis of H3K4me3 levels in WT, *hid1* and *phyB* seeds.

Supplemental Data Set 4. Gene lists summarizing ChIP-seq analysis of H3K27me3 levels in WT, *hid1* and *phyB* seeds.

Supplemental Data Set 5. *t*-test results.

Supplemental Data Set 6. Summary of mapped reads for RNA-seq, ChIP-seq, and ChIRP-seq in each of the samples.

Acknowledgments

We are grateful to Drs. Peiyong Xin and Jinfang Chu (Institute of Genetics and Developmental Biology, Chinese Academy of Sciences) for detecting the ABA and GA levels. We thank Prof. Giltsu Choi (Korea Advanced Institute of Science and Technology, Korea) for providing *PIF1OX* seeds and Dr. Xuncheng Wang for bioinformatics assistance.

Funding

This work was supported by the National Natural Science Foundation of China (grant 91940301 to D.Z.), the National Key R&D Program of China (grant 2016YFA0500800 to D.Z.), the National Natural Science Foundation of China grants (31621001 to X.W.D., 31970259 to Y.W.).

Conflict of interest statement. The authors declare no competing interest.

References

Berretta J, Morillon A (2009) Pervasive transcription constitutes a new level of eukaryotic genome regulation. EMBO Rep **10**(9): 973–982

Borthwick HA, Hendricks SB, Parker MW, Toole EH, Toole VK (1952) A reversible photoreaction controlling seed germination. Proc Natl Acad Sci U S A **38**(8): 662–666

Cho JN, Ryu JY, Jeong YM, Park J, Song JJ, Amasino RM, Noh B, Noh YS (2012) Control of seed germination by light-induced histone arginine demethylation activity. Dev Cell **22**(4):736–748

Chu C, Qu K, Zhong FL, Artandi SE, Chang HY (2011) Genomic maps of long noncoding RNA occupancy reveal principles of RNA-chromatin interactions. Mol Cell **44**(4): 667–678

Chung PJ, Park BS, Wang H, Liu J, Jang IC, Chua NH (2016) Light-Inducible MiR163 targets PXMT1 transcripts to promote seed germination and primary root elongation in arabidopsis. Plant Physiol **170**(3): 1772–1782

Clough SJ, Bent AF (1998) Floral dip: a simplified method for Agrobacterium-mediated transformation of Arabidopsis thaliana. Plant J **16**(6): 735–743

de Wit M, Galvao VC, Fankhauser C (2016) Light-mediated hormonal regulation of plant growth and development. Annu Rev Plant Biol **67**(1): 513–537

Filonov GS, Moon JD, Svensen N, Jaffrey SR (2014) Broccoli: rapid selection of an RNA mimic of green fluorescent protein by fluorescence-based selection and directed evolution. J Am Chem Soc **136**(46): 16299–16308

Gendrel AV, Lippman Z, Martienssen R, Colot V (2005) Profiling histone modification patterns in plants using genomic tiling microarrays. Nat Methods **2**(3): 213–218

He K, Cao X, Deng X (2021) Histone methylation in epigenetic regulation and temperature responses. Curr Opin Plant Biol **61**: 102001

Hu H, Du J (2022) Structure and mechanism of histone methylation dynamics in Arabidopsis. Curr Opin Plant Biol **67**: 102211

Jiang A, Guo Z, Pan J, Yang Y, Zhuang Y, Zuo D, Hao C, Gao Z, Xin P, Chu J, et al. (2021) The PIF1-miR408-PLANTACYANIN repression cascade regulates light-dependent seed germination. Plant Cell **33**(5): 1506–1529

Jiang Z, Xu G, Jing Y, Tang W, Lin R (2016) Phytochrome B and REVEILLE1/2-mediated signalling controls seed dormancy and germination in Arabidopsis. Nat Commun **7**: 12377

Kim DH, Yamaguchi S, Lim S, Oh E, Park J, Hanada A, Kamiya Y, Choi G (2008) SOMNUS, a CCCH-type zinc finger protein in Arabidopsis, negatively regulates light-dependent seed germination downstream of PIL5. Plant Cell **20**(5): 1260–1277

Lamesch P, Berardini TZ, Li D, Swarbreck D, Wilks C, Sasidharan R, Muller R, Dreher K, Alexander DL, Garcia-Hernandez M, et al. (2012) The Arabidopsis information resource (TAIR): improved gene annotation and new tools. Nucleic Acids Res **40**(D1): D1202–D1210

Langmead B, Salzberg SL (2012) Fast gapped-read alignment with bowtie 2. Nat Methods **9**(4): 357–359

Lee KP, Piskurewicz U, Tureckova V, Carat S, Chappuis R, Strnad M, Fankhauser C, Lopez-Molina L (2012) Spatially and genetically distinct control of seed germination by phytochromes A and B. Genes Dev **26**(17): 1984–1996

Li H, Handsaker B, Wysoker A, Fennell T, Ruan J, Homer N, Marth G, Abecasis G, Durbin R; 1000 Genome Project Data Processing Subgroup (2009) The sequence alignment/map format and SAMtools. Bioinformatics **25**(16): 2078–2079

Liu S, Yang L, Li J, Tang W, Li J, Lin R (2021) FHY3 Interacts with phytochrome B and regulates seed dormancy and germination. Plant Physiol **187**(1): 289–302

Liu TT, Zhu D, Chen W, Deng W, He H, He G, Bai B, Qi Y, Chen R, Deng XW (2013) A global identification and analysis of small nucleolar RNAs and possible intermediate-sized non-coding RNAs in Oryza sativa. Mol Plant **6**(3): 830–846

Liu Y, Geyer R, van Zanten M, Carles A, Li Y, Horold A, van Nocker S, Soppe WJ (2011) Identification of the Arabidopsis REDUCED DORMANCY 2 gene uncovers a role for the polymerase associated factor 1 complex in seed dormancy. PLoS One **6**(7): e22241

Liu ZW, Zhao N, Su YN, Chen SS, He XJ (2020) Exogenously overexpressed intronic long noncoding RNAs activate host gene expression by affecting histone modification in Arabidopsis. Sci Rep **10**(1): 3094

Long Y, Wang X, Youmans DT, Cech TR (2017) How do lncRNAs regulate transcription? Sci Adv **3**(9): eaao2110

Mattick JS, Taft RJ, Faulkner GJ (2010) A global view of genomic information–moving beyond the gene and the master regulator. Trends Genet **26**(1): 21–28

Oh E, Kim J, Park E, Kim JI, Kang C, Choi G (2004) PIL5, A phytochrome-interacting basic helix-loop-helix protein, is a key negative regulator of seed germination in Arabidopsis thaliana. Plant Cell **16**(11): 3045–3058

Oh E, Yamaguchi S, Hu J, Yusuke J, Jung B, Paik I, Lee HS, Sun TP, Kamiya Y, Choi G (2007) PIL5, A phytochrome-interacting bHLH protein, regulates gibberellin responsiveness by binding directly to the GAI and RGA promoters in Arabidopsis seeds. Plant Cell **19**(4): 1192–1208

Oh E, Yamaguchi S, Kamiya Y, Bae G, Chung WI, Choi G (2006) Light activates the degradation of PIL5 protein to promote seed germination through gibberellin in Arabidopsis. Plant J **47**(1): 124–139

Qu LJ, Qin G (2014) Generation and identification of Arabidopsis EMS mutants. Methods Mol Biol **1062**: 225–239

Ramirez F, Ryan DP, Gruning B, Bhardwaj V, Kilpert F, Richter AS, Heyne S, Dundar F, Manke T (2016) Deeptools2: a next generation web server for deep-sequencing data analysis. Nucleic Acids Res **44**-(W1): W160–W165

Robinson MD, McCarthy DJ, Smyth GK (2010) Edger: a bioconductor package for differential expression analysis of digital gene expression data. Bioinformatics **26**(1): 139–140

Sarkar Das S, Yadav S, Singh A, Gautam V, Sarkar AK, Nandi AK, Karmakar P, Majee M, Sanan-Mishra N (2018) Expression dynamics of miRNAs and their targets in seed germination conditions reveals miRNA-ta-siRNA crosstalk as regulator of seed germination. Sci Rep **8**(1): 1233

Seo M, Hanada A, Kuwahara A, Endo A, Okamoto M, Yamauchi Y, North H, Marion-Poll A, Sun TP, Koshiba T, et al. (2006) Regulation of hormone metabolism in Arabidopsis seeds: phytochrome regulation of abscisic acid metabolism and abscisic acid regulation of gibberellin metabolism. Plant J **48**(3): 354–366

Seo M, Nambara E, Choi G, Yamaguchi S (2009) Interaction of light and hormone signals in germinating seeds. Plant Mol Biol **69**(4): 463–472

Shi H, Wang X, Mo X, Tang C, Zhong S, Deng XW (2015) Arabidopsis DET1 degrades HFR1 but stabilizes PIF1 to precisely regulate seed germination. Proc Natl Acad Sci U S A **112**(12): 3817–3822

Shi H, Zhong S, Mo X, Liu N, Nezames CD, Deng XW (2013) HFR1 Sequesters PIF1 to govern the transcriptional network underlying light-initiated seed germination in Arabidopsis. Plant Cell **25**(10): 3770–3784

Shinomura T, Nagatani A, Chory J, Furuya M (1994) The induction of seed germination in Arabidopsis thaliana is regulated principally by phytochrome B and secondarily by phytochrome A. Plant Physiol **104**(2): 363–371

Shinomura T, Nagatani A, Hanzawa H, Kubota M, Watanabe M, Furuya M (1996) Action spectra for phytochrome A- and B-specific photoinduction of seed germination in Arabidopsis thaliana. Proc Natl Acad Sci U S A **93**(15): 8129–8133

Statello L, Guo CJ, Chen LL, Huarte M (2021) Gene regulation by long non-coding RNAs and its biological functions. Nat Rev Mol Cell Biol **22**(2): 96–118

Tamada Y, Yun JY, Woo SC, Amasino RM (2009) ARABIDOPSIS TRITHORAX-RELATED7 is required for methylation of lysine 4 of histone H3 and for transcriptional activation of FLOWERING LOCUS C. Plant Cell **21**(10): 3257–3269

Topham AT, Taylor RE, Yan D, Nambara E, Johnston IG, Bassel GW (2017) Temperature variability is integrated by a spatially embedded decision-making center to break dormancy in Arabidopsis seeds. Proc Natl Acad Sci U S A **114**(25): 6629–6634

Wang HV, Chekanova JA (2017) Long noncoding RNAs in plants. Adv Exp Med Biol **1008**: 133–154

Wang Y, Fan X, Lin F, He G, Terzaghi W, Zhu D, Deng XW (2014a) Arabidopsis noncoding RNA mediates control of photomorphogenesis by red light. Proc Natl Acad Sci U S A **111**(28): 10359–10364

Wang Y, Fan Y, Fan Z, Zhou Y, Zhang X, Wang R, Sun Y, Zhang Y, He W, Deng Y, et al. (2022) The *Arabidopsis* DREAM complex antagonizes WDR5A to modulate histone H3K4me2/3 deposition for a subset of genome repression. Proc Natl Acad Sci U S A **119**(27): e2206075119

Wang Y, Li J, Deng XW, Zhu D (2018a) Arabidopsis noncoding RNA modulates seedling greening during deetiolation. Sci China Life Sci **61**(2): 199–203

Wang Y, Luo X, Sun F, Hu J, Zha X, Su W, Yang J (2018b) Overexpressing lncRNA LAIR increases grain yield and regulates neighbouring gene cluster expression in rice. Nat Commun **9**(1): 3516

Wang Y, Wang X, Deng W, Fan X, Liu TT, He G, Chen R, Terzaghi W, Zhu D, Deng XW (2014b) Genomic features and regulatory roles of intermediate-sized non-coding RNAs in Arabidopsis. Mol Plant **7**(3): 514–527

Weitbrecht K, Muller K, Leubner-Metzger G (2011) First off the mark: early seed germination. J Exp Bot **62**(10): 3289–3309

Wierzbicki AT, Haag JR, Pikaard CS (2008) Noncoding transcription by RNA polymerase Pol IVb/Pol V mediates transcriptional silencing of overlapping and adjacent genes. Cell **135**(4): 635–648

Wu MF, Wagner D (2012) RNA In situ hybridization in Arabidopsis. Methods Mol Biol **883**: 75–86

Yang L, Jiang Z, Jing Y, Lin R (2020) PIF1 And RVE1 form a transcriptional feedback loop to control light-mediated seed germination in Arabidopsis. J Integr Plant Biol **62**(9): 1372–1384

Yu Y, Zhang Y, Chen X, Chen Y (2019) Plant noncoding RNAs: hidden players in development and stress responses. Annu Rev Cell Dev Biol **35**(1): 407–431

Zhang Y, Feng S, Chen F, Chen H, Wang J, McCall C, Xiong Y, Deng XW (2008a) Arabidopsis DDB1-CUL4 ASSOCIATED FACTOR1 forms a nuclear E3 ubiquitin ligase with DDB1 and CUL4 that is involved in multiple plant developmental processes. Plant Cell **20**(6): 1437–1455

Zhang Y, Liu T, Meyer CA, Eeckhoute J, Johnson DS, Bernstein BE, Nusbaum C, Myers RM, Brown M, Li W, et al. (2008b) Model-based analysis of ChIP-seq (MACS). Genome Biol **9**(9): R137

Zhao X, Li J, Lian B, Gu H, Li Y, Qi Y (2018) Global identification of Arabidopsis lncRNAs reveals the regulation of MAF4 by a natural antisense RNA. Nat Commun **9**(1): 5056

Zhu D, Maier A, Lee JH, Laubinger S, Saijo Y, Wang H, Qu LJ, Hoecker U, Deng XW (2008) Biochemical characterization of Arabidopsis complexes containing CONSTITUTIVELY PHOTOMORPHOGENIC1 and SUPPRESSOR OF PHYA proteins in light control of plant development. Plant Cell **20**(9): 2307–2323

Zhu P, Wang Y, Qin N, Wang F, Wang J, Deng XW, Zhu D (2016) Arabidopsis small nucleolar RNA monitors the efficient pre-rRNA processing during ribosome biogenesis. Proc Natl Acad Sci U S A **113**(42): 11967–11972